FATIGUE MODEL FOR STEEL FIBER-REINFORCED CONCRETE

Paulo B. Cachim [1], Joaquim A. Figueiras [2], and Paulo A.A. Pereira[3]

[1] *Departamento de Engenharia Civil, Universidade de Aveiro*
Campus de Santiago, 3810 AVEIRO, Portugal
[2] *Faculdade de Engenharia, Universidade do Porto*
Rua dos Bragas, 4099 PORTO CODEX, Portugal
[3] *Departamento de Engenharia Civil, Universidade do Minho*
Campus de Azurém, 4800 GUIMARÃES, Portugal

SUMMARY: A numerical model, based on the viscoplasticity theory, for the analysis of steel fiber reinforced concrete in compression is presented. The modeling of the fatigue phenomenon involves the study of a large number of cycles. Thereafter, since the modeling of the complete stress-deformation behavior is very time consuming and not suitable for the current purposes, only the increase in plastic deformation after a cycle is considered. In the current model the load is kept at a constant level and the constitutive model describes the evolution of the deformations during the cyclic load process. A series of experimental fatigue compressive tests in steel fiber reinforced concrete has been carried out to assess the model performance.

KEYWORDS: Steel fibers, fiber-reinforced concrete, viscoplasticity, compressive fatigue, fatigue modeling, concrete fatigue model.

INTRODUCTION

Concrete fatigue is a process of progressive development of small imperfections existing in the material by repetitive loads. These imperfections may be present in concrete due to concrete shrinkage, or may be caused by application of external loads. The fatigue mechanism may be attributed to progressive bond deterioration between coarse aggregates and the cement paste or by development of cracks existing in the cement paste [1, 2]. These two mechanisms may act combined or isolated, which illustrates the complexity of fatigue mechanism. The addition of fibers to concrete has a double effect on the fatigue performance of concrete. By bridging cracks, they can sustain the crack growing process providing an additional fatigue life to concrete [3-5]. On the contrary, fibers added to concrete may be cause of further defects and reduce the fatigue life of concrete [6, 7].

To understand the behavior of steel fiber-reinforced concrete under fatigue loading and to calibrate the numerical model, a series of fatigue tests carried out at the Laboratory of Structures of the Faculty of Engineering of Porto University, Portugal [7]. In these tests a sine waveform was applied between a minimum level of 10% of the monotonic strength and a maximum level ranging from 70% to 95% of the monotonic strength, at a frequency of 2.5 Hz.

Fatigue strength, *S*, is defined as the fraction of the monotonic strength that can be supported for a determined number of cycles, *N* is applied to the material. The most common way to represent fatigue data is means of a Whöler curve, where fatigue strength is plot against the number of cycles to failure. The following considerations are based on the performed experimental program. Usually a linear relation exists between fatigue strength and the logarithm of the number of cycles (Fig. 1.a). Large scatter is generally found on fatigue data and statistical methods have to be employed for data analysis. Below a stress level of 0.4 no fatigue limit was found for concrete [2] and is thus considered as the endurance limit, that is, below this stress level no fatigue failure occurs. The relation between the maximum deformation at failure and fatigue strength is shown in Fig. 1.b where an envelope for fatigue failure deformations is apparent.

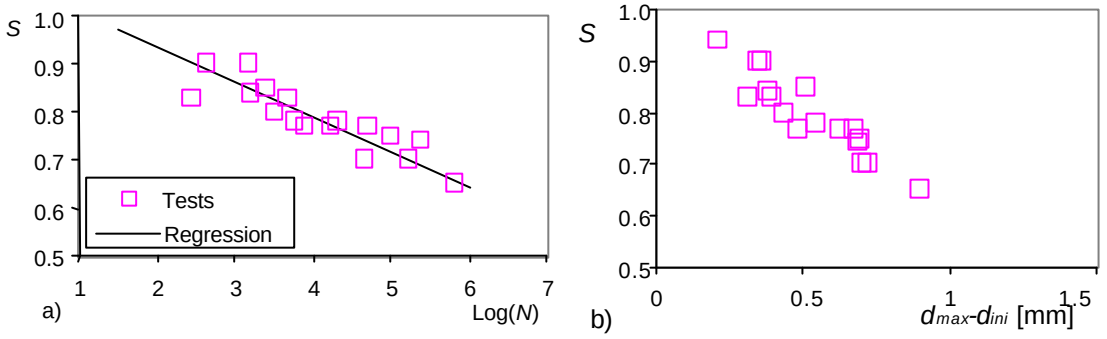

Figure 1 – Fatigue strength: a) Whöler curve and b) *d*-*S* relation.

The cyclic creep curve (Fig. 2.a) shows the evolution of the maximum deformation during a fatigue test. Clearly a linear branch can be observed during most of the test. The relation between the slope of this branch, d*e*/d*N*, and the number of cycles to failure is obviously linear when a logarithmic scale is used (Fig. 2.b). This linear relation is commonly accepted in the literature [1, 2, 9-11].

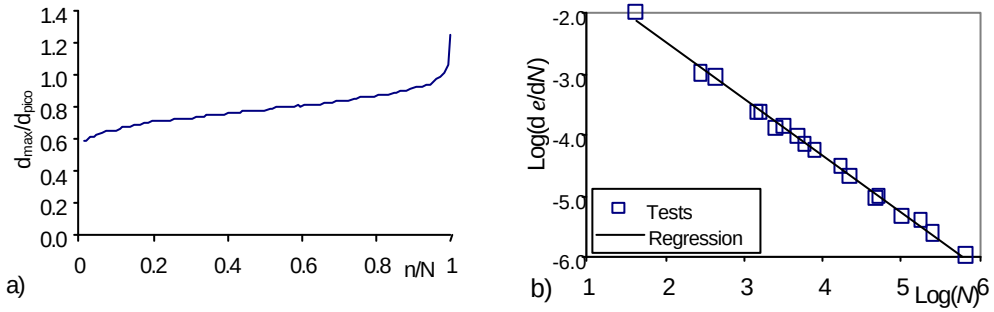

Figure 2 – Displacement evolution: a) cyclic creep curve and b) d*e*/d*N*-*N* relation.

MODEL ESSENTIALS

In this study a formulation for the study of fatigue based on viscoplasticity theory is presented. During a fatigue test, several thousands of load cycles may be necessary to cause failure in a specimen. Therefore, for such number of load cycles, it is computationally very expensive, the consideration of complete individual load/unload cycles. It is thus much more efficient the consideration of the increase in deformation per cycle, if a large number of load cycles is to be studied. In the present model, the load is kept at a constant value equal to the maximum load amplitude, while the constitutive model describes the evolution of permanent deformations [8]. An exponential law, characterized by two parameters, ζ e m controls the evolution of the permanent deformation per cycle. Permanent deformations are ruled by a surface similar to the plasticity load surface, with their direction defined by an associated law.

The developed model is based on some of the previously mentioned topics. The stress-strain relation of monotonic tests was considered as the envelope for fatigue tests, which is sustained by several authors [12, 13]. Thus, the monotonic test can be regarded as a special fatigue test where failure occurs for as single load cycle. The compressive fracture energy, G_c that rules the softening behavior has an important role in the performance of the model. The deformation velocity depends on the stress level which allows an approximately linear relation between S and log (dε/dN).

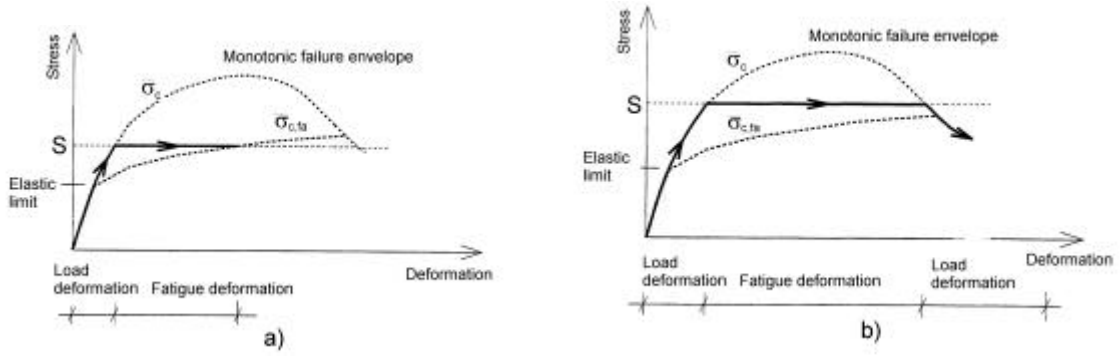

Figure 3 – Strain evolution: a) stable process and b) unstable process.

In Fig. 3 the behavior of the model for low (Fig. 3.a) and high (Fig. 3.b) stress levels is shown. The fatigue failure envelope, $\bar{\sigma}_{c,fa}$, limits the area for which there is no fatigue failure. Consequently, for a low stress level, the deformation increases until the fatigue failure envelope is reached, after what the process becomes stable. On the contrary, for a high stress level, deformation continuously increases until the monotonic failure envelope, $\bar{\sigma}_c$, is reached, after what the material becomes unstable. In this case, it is no longer possible to apply more load cycles without a reduction of the applied stress level.

A two-step procedure is employed for the fatigue analysis. First, a non-linear monotonic analysis until load reaches its maximum level (see [14] for a model description). Then, keeping the load fixed, a cycle-driven analysis is made.

CONSTITUTIVE EQUATIONS

In this section the constitutive equations of the model are presented. In the presence of relatively small deformations, the changing in deformation per cycle, $\partial \boldsymbol{e} / \partial N$, may be divided into an elastic part, $\partial \boldsymbol{e}^{e} / \partial N$, and into a plastic, permanent part, $\partial \boldsymbol{e}^{p} / \partial N$, accordingly with

$$\frac{\partial \boldsymbol{\varepsilon}}{\partial N} = \frac{\partial \boldsymbol{\varepsilon}^{e}}{\partial N} + \frac{\partial \boldsymbol{\varepsilon}^{p}}{\partial N} \tag{1}$$

where

$$\frac{\partial \boldsymbol{\varepsilon}^{e}}{\partial N} = \mathbf{D}^{-1} \frac{\partial \boldsymbol{\sigma}}{\partial N} \tag{2.1}$$

$$\frac{\partial \boldsymbol{\varepsilon}^{p}}{\partial N} = \zeta < \phi > \frac{\partial g}{\partial \boldsymbol{\sigma}} \tag{2.2}$$

where $\boldsymbol{s}$ is the stress vector, $\mathbf{D}$ is elastic constitutive matrix, $\boldsymbol{z}$ represents a measure of the deformation per cycle, $\partial g / \partial \boldsymbol{s}$ defines the direction of permanent deformations, and $<\boldsymbol{f}>$ is defined by

$$< \phi >= \begin{cases} 0, & \phi \le 0 \\ \phi = \exp\left(m \left(\dfrac{F}{F_0} - 1 \right) \right) - 1, & \phi > 0 \end{cases}$$

. (3)

The parameter m is a material characteristic. The functions g, F e F_0 depend on the state of stress and on the hardening parameter, $\boldsymbol{k}$, at the specified stress point and read

$$F(\sigma) = \left(\sigma^{T} \mathbf{P} \sigma \right)^{1/2} + \sigma^{T} \mathbf{p}(\kappa) \tag{4.1}$$

$$F_0(\kappa) = \overline{\sigma}_{c,fa}(\kappa) \tag{4.2}$$

$$g(\sigma) = F(\sigma) \tag{4.3}$$

where $\overline{s}_{c,fa}$ is the fatigue effective stress, and $\mathbf{P}$ and $\mathbf{p}$ are defined by [8]: (5)

$$\mathbf{P} = \left[\begin{array}{ccc|ccc} +1.3865 & -0.64599 & -0.64599 & & & \\ -0.64599 & +1.3865 & -0.64599 & & \mathbf{0} & \\ -0.64599 & -0.64599 & +1.3865 & & & \\ \hline & & & 4.065 & 0 & 0 \\ & \mathbf{0} & & 0 & 4.065 & 0 \\ & & & & & \end{array}\right] \qquad \mathbf{p} = \left\{\begin{array}{c} 0.1775 \\ 0.1775 \\ 0.1775 \\ 0 \\ 0 \\ 0 \end{array}\right\}$$

The fatigue effective stress function reads

$$\bar{\sigma}_{c,fa} = \begin{cases} \bar{\sigma}_{ci} + (\bar{\sigma}_{co} - \bar{\sigma}_{ci})\left(2\dfrac{\kappa}{\kappa_{co}} - \left(\dfrac{\kappa}{\kappa_{co}}\right)^2\right), & 0 < \kappa \le \kappa_{co} \\ \bar{\sigma}_{co}, & \kappa_{co} < \kappa \le \kappa_{cf} \\ \bar{\sigma}_{cr} + (\bar{\sigma}_{co} - \bar{\sigma}_{cr})\exp\left(\dfrac{\kappa}{\kappa_{cu}}\right), & \kappa_{cf} < \kappa \end{cases} \tag{6}$$

where $\bar{\sigma}_{co}$ is the yield stress value at the beginning of cyclic loading, κ_{cf} is the hardening parameter at failure, and κ_{co} and κ_{cu} are model parameters. The hardening parameter evolution is defined by

$$\frac{\partial \kappa}{\partial N} = \frac{\sigma^T \dfrac{\partial \varepsilon^p}{\partial N}}{\bar{\sigma}_{c,fa}} = \zeta < \phi > \tag{7}$$

.

NUMERICAL MODEL

The permanent deformation increment, $\Delta \varepsilon^p_{n+1}$, occurring in interval $\Delta N = N_{n+1} - N_n$ may be calculated as follows

$$\Delta \varepsilon^p_{n+1} = (1-\Theta)\frac{\partial \varepsilon^p}{\partial N_n} + \Theta \frac{\partial \varepsilon^p}{\partial N_{n+1}}, \quad 0 < \Theta < 1, \tag{8}$$

where Θ is an interpolation parameter. A expansion in series of Taylor of $\partial \varepsilon^p / \partial N_{n+1}$ leads to the following expression

$$\frac{\partial \varepsilon^p}{\partial N_{n+1}} = \frac{\partial \varepsilon^p}{\partial N_n} + \frac{\partial\left(\partial \varepsilon^p / \partial N_n\right)}{\partial \sigma_n}\Delta \sigma_n + \frac{\partial\left(\partial \varepsilon^p / \partial N_n\right)}{\partial \kappa_n}\Delta \kappa_n \tag{9}$$

where the derivatives $\partial\left(\partial \varepsilon^p / \partial N_{n+1}\right) / \partial \sigma_n$ and $\partial\left(\partial \varepsilon^p / \partial N_{n+1}\right) / \partial \kappa_n$ read

$$\frac{\partial\left(\partial \varepsilon^p / \partial N_n\right)}{\partial \sigma_n} = \mathbf{H}_n = \zeta\left[\frac{\partial \phi}{\partial \sigma_n}\left(\frac{\partial g}{\partial \sigma_n}\right) + \phi_n \frac{\partial^2 g}{\partial \sigma_n^2}\right]\Delta N$$
$$\frac{\partial\left(\partial \varepsilon^p / \partial N_n\right)}{\partial \kappa_n} = \mathbf{h}_n = \zeta\left(\frac{\partial \phi}{\partial \kappa_n}\frac{\partial g}{\partial \sigma_n} + \phi_n \frac{\partial^2 g}{\partial \kappa \partial \sigma_n}\right)\Delta N \tag{10}$$

Substituting (9) in (8) leads finally to

$$\Delta \boldsymbol{\varepsilon}^{p}_{n+1} = \left[\frac{\partial \boldsymbol{\varepsilon}^{p}}{\partial N_n} + \Theta \left(\mathbf{H}_n \Delta \boldsymbol{\sigma}_n + \mathbf{h}_n \Delta \kappa_n \right) \right] \Delta N \tag{11}$$

The evolution of the hardening parameter reads

$$\Delta \kappa_{n+1} = \frac{\partial \kappa}{\partial N_n} \Delta N = \zeta < \phi_n > \Delta N \tag{12}$$

The incremental stress-strain relation reads

$$\Delta \boldsymbol{\sigma} = \mathbf{D} \left(\Delta \boldsymbol{\varepsilon} - \Delta \boldsymbol{\varepsilon}^{p} \right) = \overline{\mathbf{D}} \Delta \boldsymbol{\varepsilon} - \Delta \mathbf{q} \tag{13}$$

where the tangent constitutive matrix, $\overline{\mathbf{D}}_n$, reads

$$\overline{\mathbf{D}}_n = \left(\mathbf{D}^{-1} + \Theta \mathbf{H}_n \Delta N \right)^{-1} \tag{14}$$

and the additional stress vector $\Delta \mathbf{q}$ is given by

$$\Delta \mathbf{q} = \left(\mathbf{D}^{-1} + \Theta \mathbf{H}_n \Delta N \right)^{-1} \left(\frac{\partial \boldsymbol{\varepsilon}}{\partial N_n} + \Theta \mathbf{h}_n \right) \Delta N \tag{15}$$

These stresses origin equivalent nodal forces, $\Delta \mathbf{f}$, accordingly to

$$\Delta \mathbf{f} = \int_V \mathbf{B}^T \Delta \mathbf{q} \, dV \tag{16}$$

where **B** is a matrix relating strains with displacements.

Box 1 shows the algorithm used for load cycle driven calculations. The integration of constitutive equations it was considered that $\Theta = 0$, which leads to an explicit integration. Consequently, the value of ΔN has to be limited in order to obtain a convergent solution. The consideration of $\Theta = 0$ origins particularly simple expressions and was used for that reason.

Box 1 – Algorithm for load cycle calculations.

Input: $\boldsymbol{\sigma}, \boldsymbol{\varepsilon}, \boldsymbol{\varepsilon}^p, \boldsymbol{\kappa}$

1. $i = 1$
2. Calculation of $\boldsymbol{f}$, $\partial g / \partial \boldsymbol{\sigma}$ and $\Delta\mathbf{q}$
3. Calculation of $\Delta\mathbf{f}$
4. if ($\|\mathbf{f}\|$ <TOLER) GOTO 11
5. if ($i = 1$) $\mathbf{K} = \int_V \mathbf{B}^T \mathbf{D}\, \mathbf{B}\, dV$
6. $\Delta d = \mathbf{K}^{-1}\Delta\mathbf{f}$
7. Calculation of $\Delta\boldsymbol{\sigma}$
8. Calculation of $\Delta\boldsymbol{\kappa}$
9. Actualization of $\boldsymbol{\sigma}$ and $\boldsymbol{\kappa}$
10. $i = i+1$, GOTO 2
11. END

NUMERICAL EXAMPLES

Two application examples are presented. In the first one, the results of the numerical model are compared with the experimental data. The second example compares the results of model with the results of the biaxial fatigue tests of Yin and Hsu [5] for fiber-reinforced concrete. Isoparametric plane finite elements are used with reduced integration on 2x2 Gauss points and dimensions of 100x100x100 mm^3.

Comparison with experimental results

This section deals with the ability of the model to simulate experimental results. The model was compared with data acquired from compressive fatigue tests on cylinders [7]. Concrete properties and model parameters are presented in Table 1. These properties are attained from comparison of monotonic experiment data with model behavior (Fig. 4)

Table 1 – Concrete properties for numerical analysis.

Properties	Value	Units	Properties	Value	Units
E_c	30000	N/mm^2	υ	0.15	-
f_c	52	N/mm^2	G_c	7	N/mm
m	5	-	$\boldsymbol{\zeta}$	$2x10^{-5}$	-

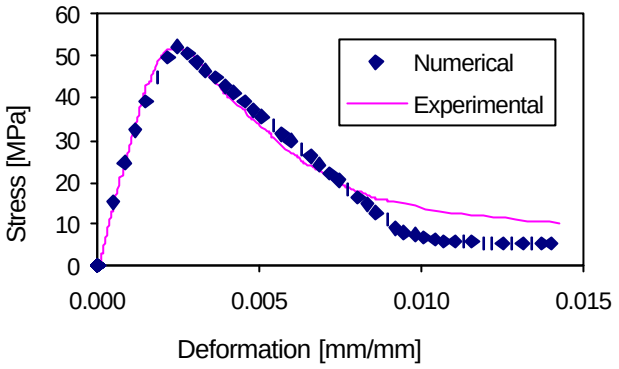

Figure 4 – Model results: monotonic stress-strain diagram.

The S-N diagram obtained with the model is shown in Fig. 5 where experimental data is also plotted.

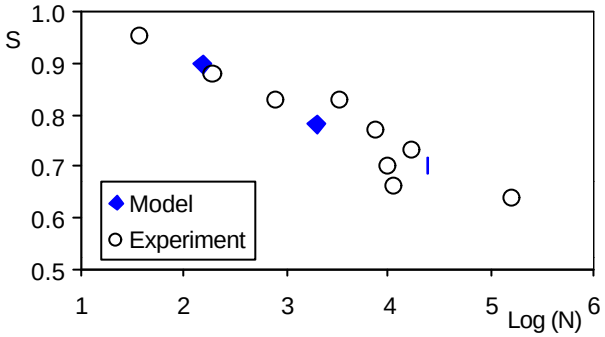

Figure 5 – S-N diagram for model and experimental results.

The imporatant relation between $\log(d\varepsilon/dN)$ and N is plotted in Fig. 6. As can be seen, good agreement is found between the results of the numerical model and experimental results.

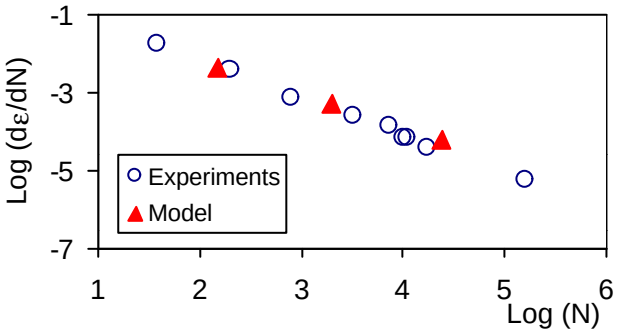

Figure 6 – Relation between dε/dN and N.

Biaxial compression

To assess the model performance under biaxial conditions, the presented model is compared with the results of Yin and Hsu [5]. Fig. 7 illustrates both results.

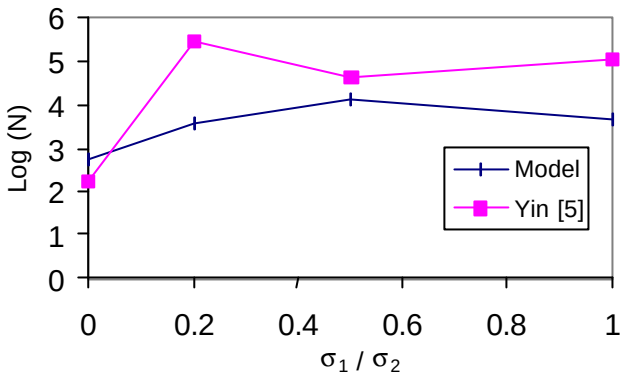

Figure 7 – Relation between dε/d*N* and N.

It can be seen that a satisfactory agreement is found, although the numerical model underestimates the biaxial fatigue life. Unfortunately, there is not very information about the biaxial fatigue behavior of concrete in order to improve the behavior of the model.

CONCLUSIONS

A numerical model for the analysis of fiber reinforced concrete under compressive fatigue has been developed. A series of compressive fatigue tests on cylinders have been carried out to understand the behavior of fiber reinforced concrete under fatigue and to allow the model calibration.

Regardless of relatively model simplicity, through adequate characterization of the parameters ***z***, *m* e G_c, it is possible to attain a good representation of experimental results. The biaxial behavior of the model is not so impressive although satisfactory agreement between numerical and experimental results is attained.

ACKNOWLEDGEMENTS

The authors wish to express their gratitude to the firms BEAKAERT Portugal, SECIL, MBT Portugal, SEOP, TRIQUIMICA, and FAPREL for the support given to the current research program.

REFERENCES

1. RILEM, “Long term random dynamic loading of concrete structures”, Materiaux et Constructions, Vol. 17, nº 97, 1984, pp. 1-27.

2. CEB, “Fatigue of concrete structures - state of the art report”, Bulletin d'Information nº 188, 1988.

3. Ramakrishnan, V. *et al*., “Cyclic behavior, fatigue strength, endurance limit and models for fatigue behavior of FRC”, High Performance Fiber Reinforced Cement Composites 2, Ed. Naaman and Reinhardt, E & FN Spon, London, 1996.

4. Paskova, T. and Meyer, C., “Low-cycle fatigue of plain and fiber-reinforced concrete”, ACI Mat. Journal, July-Aug., 1997, pp.273-285.

5. Yin W.S. and Hsu, T.C., "Fatigue behavior of steel fiber reinforced concrete in uniaxial and biaxial compression", ACI Materials Journal, Vol. 92, nº 1, 1995, pp.71-81.

6. Grzybowski, M. and Meyer, C., “Damage accumulation in concrete with and without fiber reinforcement”, ACI Mat. Journal, Nov.-Dec., 1993, pp.594-604.

7. Cachim, P.B., Figueiras, J.A. and Pereira, P.A.P., “Effects of long steel fibres on the fatigue life of concrete” – to be published, Int. Conf. On Infrast. Regener. And Rehabil., Sheffield, U.K., 1999.

8. Suiker, A.S.J.; de Borst, R., “Low-cycle fatigue of granular materials”, Computational Plasticity, Eds. Owen, Oñate & Hinton, CIMNE, Barcelona, Espanha, 1997, pp. 1729-1736.

9. Hordijk D.A. *et al*, “Fracture and fatigue behaviour of high strength limestone concrete as compared to gravel concrete”, HERON, Vol. 40, nº 2, 1995, pp. 125-146.

10. Nelson, E.L., Carrasquillo, R.L. and Fowler, D.W., “Behavior and failure of high-strength concrete subjected to biaxial-cyclic compression loading”, ACI Materials Journal, Vol. 85, nº 3, 1988, pp.248-253.

11. Taliercio, A.L.F. and Gobbi, E., “Experimental investigation on the triaxial fatigue behavior of plain concrete”, Mag. of Concr. Res., Vol. 48, nº 176, 1996, pp. 157-172.

12. Karsan, I.D.; Jirsa, O. “Behaviour of concrete under compressive loadings” *J. St. Divis. ASCE*, Vol. 95, 1969, pp. 2543-2563.

13. Otter, D.E.; Naaman, A.E., “Properties of steel fiber reinforced concrete under cyclic loading”, ACI Materials Journal, 1989, pp.254-261.

14. Cachim, P.B. *et al*, “Modelo elastoplástico para o betão sob estados de tensão multiaxiais”, in portuguese, V Enc. Nac. Mec. Comp. Guimarães, Portugal, 1997, pp. 261-270.